This paper describes objective technical results and analysis. Any subjective views or opinions that might be expressed in the paper do not necessarily represent the views of the U.S. Department of Energy or the United States Government.

SAND2019-4833J

High-Gain Leaky Surface Acoustic Wave Amplifier in Epitaxial InGaAs on Lithium Niobate Heterostructure

L. Hackett,[1] A. Siddiqui,[1] D. Dominguez,[1] J. K. Douglas,[1] A. Tauke-Pedretti,[1] T. Friedmann,[1] G. Peake,[1] S. Arterburn,[1] and M. Eichenfield[1,a)]

[1]*Sandia National Laboratories, Albuquerque, NM, 87123, USA*

Active surface acoustic wave components have the potential to transform RF front ends by consolidating functionalities that currently occur across multiple chip technologies, leading to reduced insertion loss from converting back and forth between acoustic and electronic domains in addition to improved size and power efficiency. This letter demonstrates a significant advance in these active devices with a compact, high-gain, and low-power leaky surface acoustic wave amplifier based on the acoustoelectric effect. Devices use an acoustically thin semi-insulating InGaAs surface film on a YX lithium niobate substrate to achieve exceptionally high acoustoelectric interaction strength via an epitaxial $In_{0.53}Ga_{0.47}As(P)/InP$ quaternary layer structure and wafer-scale bonding. We demonstrate 1.9 dB of gain per acoustic wavelength and power consumption of 90 mW for 30 dB of electronic gain. Despite strong intrinsic leaky propagation loss, 5 dB of terminal gain is obtained for a semiconductor only 338 microns long due to state-of-the-art heterogenous integration and an improved material platform.

[a)] Electronic mail: meichen@sandia.gov.

RF devices are becoming more multi-band, increasing the number of filters and other front-end components while simultaneously pushing towards reduced cost, size, weight, and power (CSWaP). One approach to reducing CSWaP is to eliminate high quality factor filtering that relies on acoustic wave technologies,[1] allowing end-to-end solutions in CMOS or compound semiconductor platforms. Another way would be to augment the achievable functionalities of electromechanical/acoustic filtering chips to include "active" and nonlinear functionalities, such as gain and mixing. The acoustoelectric (AE) effect could enable such active acoustic wave devices, but, to compete with the performance of today's multi-chip architectures, any solution to this problem needs to provide high gain, large bandwidth, low noise figure, and sufficient power handling, in addition to the reduced CSWaP.

Surface acoustic wave (SAW) amplifiers based on the AE effect were demonstrated as early as the 1960s.[2] In these devices, evanescent fields associated with piezoelectric acoustic waves interact with charge carriers undergoing voltage-induced drift. The interaction causes polarization of the drifting majority charge carriers that leads to a Coulomb drag effect, resulting in acoustic wave attenuation or amplification,[3] analogous to a traveling-wave tube amplifier.[4] The expected loss per radian α/k_0 can be described by an intuitive model that treats the system as an RC circuit:[5]

$$\frac{\alpha}{k_0} = \frac{1}{2} k_{AE}^2 \frac{\gamma\omega\tau}{1 + (\gamma\omega\tau)^2} \quad (1)$$

where k_{AE}^2 is an effective electromechanical coupling coefficient between the drifting carriers and the piezoelectric wave, k_0 is the acoustic wave number, $\gamma = (1 - v_d/v_s)$, $v_d = \mu E$ is the carrier drift velocity, μ is the carrier mobility, E is the electric field, and v_s is the SAW velocity. The value of k_{AE}^2 is equivalent to the SAW substrate electromechanical coupling coefficient $k^2 = 2\Delta v/v_f$ where $\Delta v = v_f - v_m$ is the difference between the acoustic velocities v_f and v_m for the open (free) and short (metallized) boundary conditions, respectively. For an acoustically thin film, $\tau = (\varepsilon + \varepsilon_0)/\sigma k_0 t$ where ε is the piezoelectric material permittivity, ε_0 is the vacuum permittivity, σ is the semiconductor conductivity, and t is the semiconductor thickness.[5]

The amplifier performance is improved by utilizing a piezoelectric substrate with a large k_{AE}^2, which alone determines the *maximum* α/k_0, combined with a semiconductor with small σt and high μ to lower the required voltage for a given gain.[5] Previous demonstrations of SAW amplifiers have resulted in over 100 dB of RF output contrast (a.k.a. *electronic* gain), but at voltages exceeding 1 kV.[6-11] Molecular beam epitaxy (MBE) and metal-organic chemical vapor deposition (MOCVD) were either in their infancy or not yet invented, making it impossible, at the time, to seamlessly integrate low defectivity semiconductors with small σt and high μ with large k^2 piezoelectric substrates.

AE amplifiers consisted of essentially one of two types: 1) evaporated thin semiconductor layers with large σ and high defectivity on piezoelectric substrates or 2) bulk crystalline semiconductors separated from the piezoelectric by a thin air gap to prevent acoustic radiation into the thick semiconductor. The first approach yielded performance limited by the sub-optimal material properties; the second approach significantly reduced the AE interaction strength and made the devices more dispersive, which prevents high frequency operation. Other implementations use charge confinement structures or the high μ of 2D materials, but

Sandia National Laboratories is a multimission laboratory managed and operated by National Technology & Engineering Solutions of Sandia, LLC, a wholly owned subsidiary of Honeywell International Inc., for the U.S. Department of Energy's National Nuclear Security Administration under contract DE-NA0003525.

performance of these devices has never approached that of the other two.[12]

In this letter, we present a high gain leaky SAW (LSAW) amplifier based on heterogenous integration of an epitaxial III-V semiconductor and lithium niobate ($LiNbO_3$), providing a solution to the aforementioned problems and enabling compact, high-gain devices with significantly lower power consumption. YX $LiNbO_3$ is chosen due to its exceptionally high k^2 (~25%), providing the highest k_{AE}^2 for a SAW on bulk $LiNbO_3$.[13] We demonstrate *acoustic* gain of 1.9 dB/Λ in a 338 µm long device, where Λ is the acoustic wavelength, equivalent to an *electronic* gain of 30.3 dB and a *terminal* gain of 5 dB. Moreover, on account of the directly bonded semiconductor layer's low σt and relatively high μ, this large peak gain occurs at only -55 V.

Figure 1 illustrates the LSAW amplifier at various scales. As shown in the schematic in Fig. 1(a), the device consists of an acoustically thin InGaAs epitaxial film in a YX $LiNbO_3$ delay line with integrated RF and DC contacts. The lattice-matched $In_{0.53}Ga_{0.47}As(P)/InP$ epitaxial stack that yields the amplifier film, grown by MOCVD, is shown in Fig. 1(b). To fabricate the amplifiers, the InP wafer is bonded to the $LiNbO_3$ wafer with the epitaxial stack layers in direct contact with the $LiNbO_3$. The final structure consists of a 100 nm thick InGaAs amplifier layer with a target doping concentration (N_D) of $6x10^{15}$ cm^{-3} separated from the $LiNbO_3$ by a 2 nm thick non-intentionally doped (NID) InP layer. Quasi-ohmic DC contact is made to the InGaAs by depositing an Au/Ag metal stack on two patterned 100 nm InP layers doped at $5x10^{16}$ cm^{-3} and $5x10^{18}$ cm^{-3}. Atomic force microscope scans, such as the one shown in Fig. 1(c), evaluated the epitaxial surface to have a low defectivity and rms roughness. This enabled amplifiers, such as the one shown in the optical microscope images in Fig. 1(d) and Fig. 1(e) to be fabricated over the 2 inch InP wafer with over 75% yield (Fig. 1(f)).

Despite high k^2, YX $LiNbO_3$ is rarely utilized due to bulk wave radiation leading to propagation losses for the short and open boundary conditions of approximately α_m = 0.5 dB/Λ and α_f = 0.25 dB/Λ, respectively.[11] However, increased need for a higher k^2 and the corresponding larger bandwidth has led to studies of 0-15° YX $LiNbO_3$ with the objective to reduce the attenuation.[13-15] Here we demonstrate that despite typical strong attenuation, we obtain large gains in YX $LiNbO_3$ InGaAs LSAW amplifiers due to the high k_{AE}^2 and optimized material platform. Whether the amplifier produces gain depends on the applied bias and the contribution of the LSAW's intrinsic propagation loss to the AE effect. Without LSAW propagation loss, there is gain when $v_d > v_s$ and loss when $v_d < v_s$ such that an applied synchronous drift voltage $V_{syn} = v_s l/\mu$ results in $\alpha/k_0 = 0$. As shown in Fig. 1(g), when there is no drift voltage applied to the semiconductor, the LSAW is attenuated further than its intrinsic value due to the AE interaction. For LSAW amplification, as shown in Fig. 1(h), the synchronous condition must be met, and the gain must be large enough to overcome leaky propagation loss.

A schematic of the experimental setup utilized for gain measurements is shown in Fig. 2(a). To avoid complications from thermal drift and run-away, which can corrupt gain measurements and even destroy the devices, the amplifier is operated in a pulsed mode. The S_{21} value at the operating frequency is measured with respect to time during the application of a 1 ms voltage pulse. The current is simultaneously monitored across a shunt resistor. The RF transducer has a 2 mm aperture, 6 finger pairs, and a finger pitch of 10.57 µm; a resonance occurs at 205 MHz, corresponding to an acoustic wave velocity of 4334 m/s, which agrees well with the expected YX LSAW velocity.[16] The gain or loss relative to 0 V ($S_{21}(V_{on})$-$S_{21}(V_{off})$) where $S_{21}(V_{on})$ and $S_{21}(V_{off})$ denote the S_{21} signal with the voltage pulse on and off, respectively, is shown in Fig. 2(b). We obtain 39.8 dB (1178 dB/cm) of gain relative to the 0 V level. The IV curve in Fig. 2(c) shows a nonlinear relationship between current and applied bias. This is likely due to a strain-induced, voltage-dependent modification of the semiconductor band structure near the DC contacts due to the proximity of the piezoelectric substrate, which has been described in other works.[17]

A gain pulse at a drift field of -1.63 kV/cm, corresponding to an applied bias of -55 V, is shown in Fig. 3(a), yielding a terminal gain of 5 dB for the 338 µm long amplifier. In addition, after the voltage pulse ends, the S_{21} signal returns to

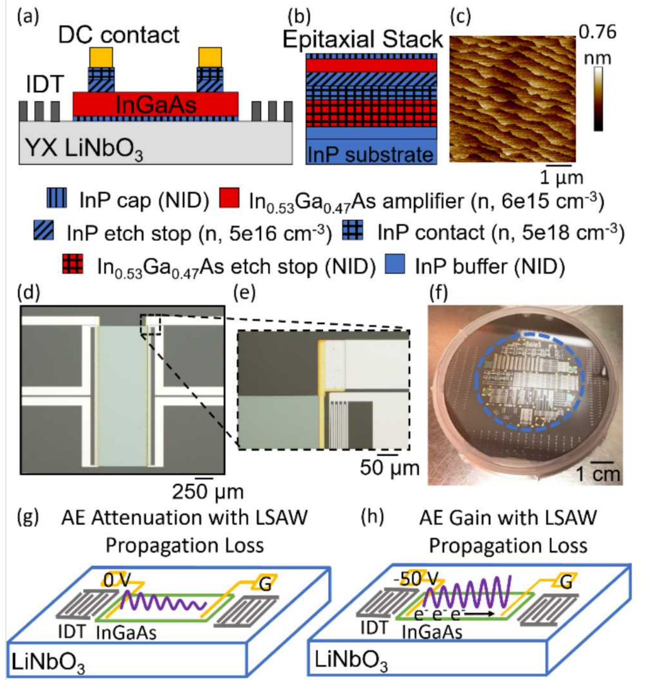

FIG. 1. (a) A cross-sectional schematic of the device, which consists of a 100 nm thick InGaAs layer with DC contacts integrated in a YX $LiNbO_3$ delay line. (b) Schematic and (c) atomic force microscope scan of the initial epitaxial stack before bonding to the $LiNbO_3$ and further processing. (d) Microscope image of the fabricated device with (e) an image of the interdigital transducers and DC contact. (f) Camera image of the 3 inch $LiNbO_3$ wafer after fabricating arrays of devices. The bonded 2 inch InP wafer is indicated by the dashed blue line. The expected amplifier response with (g) no applied bias and (h) a drift voltage sufficient for gain.

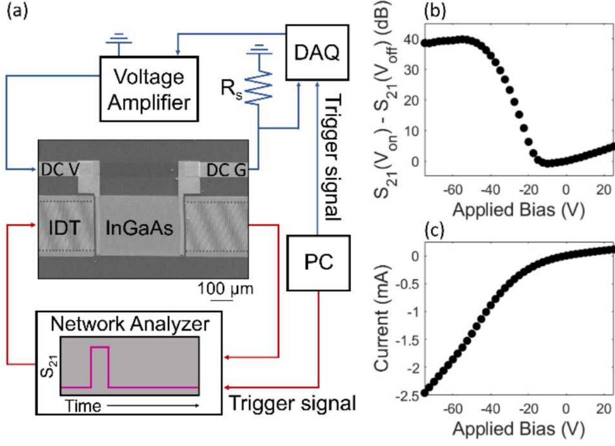

FIG. 2. (a) The experimental setup for gain measurements is shown. S_{21} is recorded with respect to time as a voltage pulse is applied. Collected experimental data showing the (b) relative S_{21} value and (c) IV curve.

its original baseline value, indicating negligible levels of hysteresis and time-dependent drift (e.g., thermal). The amplifier shows 35 dB of insertion loss at 0 V. This is a combination of AE attenuation, propagation losses, and transducer conversion losses.

Electronic gain in dB/cm is plotted as a function of drift field in Fig. 3(b). The values for μ, N_D, k_{AE}^2, α_f, and α_m are obtained from the experimental gain curve. To add the contribution of LSAW propagation loss to Eqn. (1), we follow previous derivations for the AE effect in semiconductor on piezoelectric monolithic geometries.[5,18,19] For LSAW, v_m and v_f are complex such that $v_m = v_{mr} + iv_{mi}$ and $v_f = v_{fr} + iv_{fi}$ where the subscript r denotes the real component and the subscript i denotes the imaginary component. This modifies the piezoelectric impedance,[18] which, in turn, modifies the expected relative change in wave number due to the semiconductor layer. The modified expression for α/k_0 is then:

$$\frac{\alpha}{k_0} = \frac{1}{2}k_{AE}^2\frac{\gamma\omega\tau}{1+(\gamma\omega\tau)^2} + \frac{v_{mi}}{v_{fr}}\frac{(\gamma\omega\tau)^2}{1+(\gamma\omega\tau)^2} + \frac{v_{fi}}{v_{fr}}\frac{1}{1+(\gamma\omega\tau)^2}. \quad (2)$$

According to Eqn. (2), V_{syn} is determined by the peak slope of the gain curve. Using this method, we find μ=732 cm²/V-s, which is significantly lower than the bulk InGaAs value of 10,000 cm²/ V-s, but this decrease is expected for a 100 nm thick film integrated into an AE device and can be improved in future studies with surface passivation.[20]

We do not fit the data to the model in the peak gain or attenuation regions, but instead consider α/k_0 near V_{syn}. While a decrease in gain at large negative drift fields, is expected from Eqn. (2), modeling in this region is complicated by thermal effects and other large signal behavior, which we have not included in the small signal model presented here. In addition, the data in the attenuation region is strongly limited by bulk mode excitation.[21] The bulk modes exist in the substrate instead of on the surface and therefore are not amplified or attenuated, leading to a constant background. Taking the case where $\gamma\omega\tau \ll 1$, Eqn. (2) reduces to:

$$\frac{\alpha}{k_0} = \frac{1}{2}k_{AE}^2\gamma\omega\tau + \frac{v_{mi}}{v_{fr}}(\gamma\omega\tau)^2 + \frac{v_{fi}}{v_{fr}}. \quad (3)$$

The LSAW contribution is voltage-dependent, nonlinear, and results in a modified voltage V_0 to obtain $\alpha/k_0 = 0$ given by $V_0 = V_{syn} + V_l$ where V_l is the additional voltage required to overcome the contribution of leaky propagation loss.

We utilize a nonlinear least squares fit of the experimental gain curve data points around V_{syn} to Eqn. (3) to obtain N_D, k_{AE}^2, α_f, and α_m. V_0 is determined using μ=732 cm²/V-s, and the fitted value for α_f immediately follows. The coefficients k_{AE}^2 and α_m vary depending on the initial N_D; for example, setting $N_D = 6\times10^{15}\text{cm}^{-3}$, we obtain $k_{AE}^2 = 28\%$, which is unphysical, since k_{AE}^2 would be larger than k^2. Clearly, the actual N_D is less than the value targeted for epitaxy. With an upper bound on k_{AE}^2 of 25%, the coefficients N_D, k_{AE}^2, and α_f are $(5.2\pm0.2)\times10^{15}\text{cm}^{-3}$, $(24\pm4)\%$, and (0.2 ± 0.1) dB/Λ, respectively. The parameter α_m has a small contribution at low gain leading to an unreasonable uncertainty from the fitting. Based on this analysis, a gain of 896 dB/cm is obtained at a drift field of -1.63 kV/cm. The fit and experimental data points used are indicated in Fig. 3(b). We also examined the large signal power saturation characteristics of the amplifier, which occur due to limited space-charge modulation.

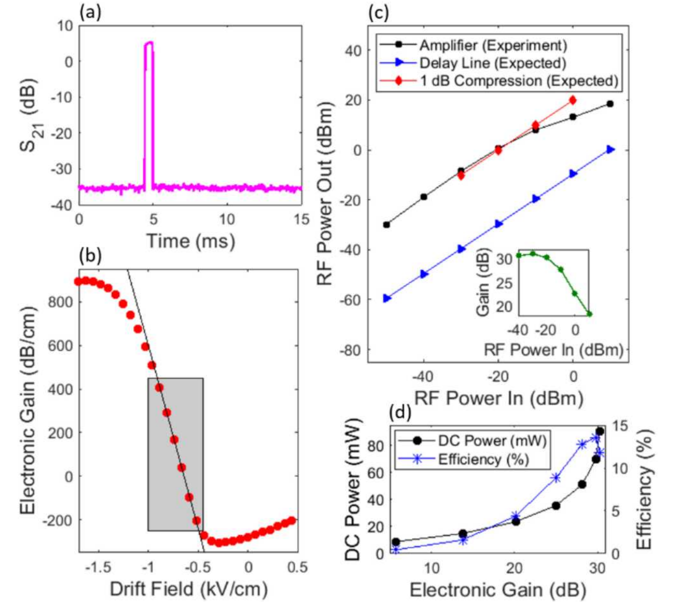

FIG. 3. (a) The measured gain pulse is shown at an applied bias of -55 V. Terminal gain of 5 dB is obtained. (b) Electronic gain in dB/cm is plotted as a function of the drift field. The black line is the gain expression from Eqn. (3) and the gray box indicates the experimental data points used for the fitting. (c) The RF power output is plotted as a function of RF power input for the amplifier device. Also shown for comparison is the expected RF output power for a LSAW delay line and a LSAW amplifier with 1 dB of gain compression. The inset shows the gain value as a function of increasing RF input power. (d) DC power consumption and efficiency are plotted as a function of the electronic gain.

TABLE I. LSAW amplifier performance compared to notable works.

Material System	k_{AE}^2 *(%)*	*Freq. (MHz)*	*Gain (dB/cm)*	*Gain (dB/Λ)*	*t (nm)*	*ρ (Ω-cm)*	*Power (W)*	*Reference*
InGaAs/YX $LiNbO_3$	24	205	896	1.9	100	1.98	0.09	This work
InSb/YZ $LiNbO_3$	4.6	670	92	0.05	55	0.092	12.9	[9]
InSb/41° YX $LiNbO_3$	17.2	160	40	0.11	100	0.1	14.6	[10]
Si/YZ $LiNbO_3$	4.6	100	55	0.18	800	8	8	[7]

In Fig. 3(c), the RF power output is plotted as a function of the RF power input, assuming 9.6 dB of propagation loss (0.6 dB/Λ) that is determined by a 3D FEM model of the YX $LiNbO_3$ delay line with an infinite aperture and 100 nm semiconductor film. Only the mechanical properties of the semiconductor are considered in the model. Considering propagation loss and 9.5 dB of loss due to the AE effect, as determined by the previous fit to the gain curve, the remaining 15.9 dB of insertion loss is assigned to the transducers. Also shown for comparison in Fig. 3(c) is the expected RF output power for the delay line with no semiconductor and for an amplifier with 1 dB of gain compression. The 1 dB gain compression point for this amplifier occurs at 3.6 dBm.

In Fig. 3(d), the DC power consumption and the power efficiency $\eta = P_{OUT}^{RF}/P_{IN}^{DC}$ are plotted as a function of the electronic gain where P_{OUT}^{RF} is the RF output power and P_{IN}^{DC} is the DC input power. At the peak gain of 30.3 dB, the required DC power is 90.4 mW, resulting in $\eta = 1.3\%$. In general, optimizing η is nontrivial because it depends on σt, gain, and the power handling capabilities of the device.

To assess the performance of the LSAW amplifier reported here, we compare our results with those from previous notable AE amplifier demonstrations in Table I. The electronic gain normalized to the wavelength (dB/Λ) gives a frequency-independent comparison between amplifiers. To compare power consumption, the device lengths and corresponding drift voltages from the referenced works were normalized to correspond to 30 dB of electronic gain. Based on these values, our material platform has at least a 10X performance improvement in terms of electronic gain in dB/Λ and at least an 89X improvement in the power required to obtain 30 dB of electronic gain.

YX $LiNbO_3$ was used as the piezoelectric substrate in this work due to its high k^2. However, the intrinsic LSAW propagation loss degrades performance. While it can be reduced by methods such as mass loading,[14] there are also LSAW cuts with lower k^2, but significantly lower attenuation.[16] Figure 4 shows simulated YX SAW and LSAW v_f and v_m (Fig. 4(a)), k^2 (Fig. 4(b)), and α_f and α_m (Fig. 4(c)) for X-propagation with changing Y-cut angle. The slow shear bulk wave (SSBW) and fast shear bulk wave (FSBW) velocities are also indicated in Fig. 4(a). As expected, k^2 is maximized with 0° YX $LiNbO_3$. However for 41° YX, k^2 remains high at 17.5%, and $\alpha_f = 0$. Another known LSAW cut is 64° YX where we obtain a k^2 of 11.4% and $\alpha_m = 0$.

Taking into consideration early roll-over in the gain curves and propagation losses, with unidirectional and impedance matched transducers we would expect approximately 21 dB,

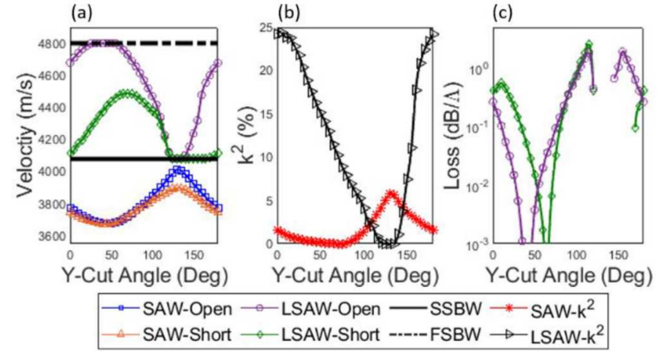

FIG. 4. Simulated values for the SAW and LSAW (a) velocities in addition to the (b) k^2 values and (c) propagation losses for X-propagation and changing Y-cut angle.

22 dB, and 10 dB of *terminal* gain for 0°, 41°, and 64° YX $LiNbO_3$, respectively at an applied bias of -55 V and power requirement of 90 mW. In future studies, the tradeoff between k^2 and propagation loss will be experimentally evaluated to obtain the maximum terminal gain.

We have presented a LSAW amplifier with high gain and low power consumption enabled by high k^2, small σt, relatively high μ for a thin, unpassivated film, and state-of-the art wafer-scale bonding and fabrication. However, in addition to combating intrinsic LSAW propagation loss, several challenges remain to make active SAW devices based on the AE effect competitive with existing multichip RF front-end technologies. This includes employing device geometries with improved heat dissipation to enable the devices to run continuously and demonstrating operation at higher frequencies. The noise figure is another crucial component of device performance that will be examined in detail in future studies. An amplifier based on a SAW delay line could have an immediate impact in the receive signal chain of a RF front end module by reducing the need for external low-noise amplifiers. The results reported in this letter suggest that the $LiNbO_3$ LSAW and III-V epitaxial semiconductor material platform can serve as a building block for more advanced active RF acoustic devices.

Supported by the Laboratory Directed Research and Development program at Sandia National Laboratories, a multimission laboratory managed and operated by National Technology and Engineering Solutions of Sandia, LLC., a wholly owned subsidiary of Honeywell International, Inc., for the U.S. Department of Energy's National Nuclear Security Administration under contract DE-NA-003525. This paper describes objective technical results and analysis. Any

subjective views or opinions that might be expressed in the paper do not necessarily represent the views of the U.S. Department of Energy or the United States Government.

REFERENCES

[1] D. Kaczman, M. Shah, M. Alam, M. Rachedine, D. Cashen, L. Han, and A. Raghavan, IEEE J Solid-St Circ **44** (3), 718 (2009).

[2] J. H. Collins, K. M. Lakin, C. F. Quate, and H. J. Shaw, Appl Phys Lett **13** (9), 314 (1968); K. M. Lakin and H. J. Shaw, IEEE T Microw Theory **Mt17** (11), 912 (1969).

[3] M. Rotter, A. Wixforth, W. Ruile, D. Bernklau, and H. Riechert, Appl Phys Lett **73** (15), 2128 (1998); W. C. Wang, Phys Rev Lett **9** (11), 443 (1962); G. Weinreich, T. M. Sanders, and H. G. White, Phys Rev **114** (1), 33 (1959); G. Weinreich and H. G. White, Phys Rev **106** (5), 1104 (1957).

[4] R. Kompfner, P Ire **35** (2), 124 (1947).

[5] R. Adler, IEEE T Son Ultrason **Su18** (3), 115 (1971).

[6] G. Cambon, M. Rouzeyre, and C. Fournier, Electron Lett **8** (3), 60 (1972).

[7] S. H. Chisholm, P IEEE **57** (4), 740 (1969).

[8] L. A. Coldren and G. S. Kino, Appl Phys Lett **18** (8), 317 (1971).

[9] L. A. Coldren and G. S. Kino, IEEE T Electron Dev **Ed21** (7), 421 (1974).

[10] J. Henaff and M. Feldmann, Appl Phys Lett **24** (9), 447 (1974).

[11] K. Yamanouchi and K. Shibayama, J Appl Phys **43** (3), 856 (1972).

[12] Z. Insepov, E. Emelin, O. Kononenko, D. V. Roshchupkin, K. B. Tnyshtykbayev, and K. A. Baigarin, Appl Phys Lett **106** (2) (2015); L. Shao and K. P. Pipe, Appl Phys Lett **106** (2) (2015); H. S. Zhu and M. Rais-Zadeh, IEEE Electr Device L **38** (6), 802 (2017).

[13] K. Hashimoto, H. Asano, T. Omori, and M. Yamaguchi, Jpn J Appl Phys 1 **43** (5b), 3063 (2004).

[14] J. Koskela, V. P. Plessky, and M. T. Salomaa, IEEE T Ultrason Ferr **45** (2), 439 (1998).

[15] K. Yamanouchi and T. Ishii, Japanese Journal of Applied Physics Part 1-Regular Papers Brief Communications & Review Papers **41** (5b), 3480 (2002).

[16] A. Takayanagi, K. Yamanouchi, and K. Shibayama, Appl Phys Lett **17** (5), 225 (1970).

[17] A. Piyadasa, S. B. Wang, and P. X. Gao, Semicond Sci Tech **32** (7) (2017); J. Shi, M. B. Starr, and X. D. Wang, Adv Mater **24** (34), 4683 (2012); Y. Zhang, Y. Liu, and Z. L. Wang, Adv Mater **23** (27), 3004 (2011); Z. C. Zhang, L. K. Li, J. Horng, N. Z. Wang, F. Y. Yang, Y. J. Yu, Y. Zhang, G. R. Chen, K. Watanabe, T. Taniguchi, X. H. Chen, F. Wang, and Y. B. Zhang, Nano Lett **17** (10), 6097 (2017).

[18] K. A. Ingebrigtsen, J Appl Phys **40** (7), 2681 (1969).

[19] K. A. Ingebrigtsen, J Appl Phys **41** (2), 454 (1970); K. Yamanouchi, K. Abe, and K. Shibayama, IEEE T Son Ultrason **22** (5), 369 (1975).

[20] T. P. Pearsall and J. P. Hirtz, J Cryst Growth **54** (1), 127 (1981).

[21] T. I. Browning and M. F. Lewis, Electron Lett **13** (5), 128 (1977); N. H. C. Reilly, R. F. Milsom, and M. Redwood, Electron Lett **9** (18), 419 (1973); Y. W. Zhang and M. Planat, Electron Lett **23** (2), 68 (1987).